



Article

# THz Range Low-Noise SIS Receivers for Space and Ground-Based Radio Astronomy <sup>†</sup>

Kirill I. Rudakov <sup>1,2</sup>, Andrey V. Khudchenko <sup>1,3</sup> , Lyudmila V. Filippenko <sup>1</sup>, Maxim E. Paramonov <sup>1</sup>, Ronald Hesper <sup>2</sup>, Daniele Aragão Ronsó da Costa Lima <sup>2,4</sup>, Andrey M. Baryshev <sup>2</sup>  and Valery P. Koshelets <sup>1,3,\*</sup>

<sup>1</sup> Kotelnikov Institute of Radio Engineering and Electronics of Russian Academy of Sciences, Mokhovaya 11-7, 125009 Moscow, Russia; k.rudakov@astro.rug.nl (K.I.R.); khudchenko@asc.rssi.ru (A.V.K.); lyudmila@hitech.cplire.ru (L.V.F.); paramonov@hitech.cplire.ru (M.E.P.)

<sup>2</sup> Kapteyn Astronomical Institute, University of Groningen, 9712 CP Groningen, The Netherlands; r.hesper@astro.rug.nl (R.H.); daniele.ronso@usp.br (D.A.R.d.C.L.); andrey@astro.rug.nl (A.M.B.)

<sup>3</sup> Astro Space Center of Lebedev Physical Institute of Russian Academy of Sciences, 117810 Moscow, Russia

<sup>4</sup> Instituto da Astronomia, University of São Paulo, Rua do Matão, São Paulo 1226, Brazil

\* Correspondence: valery@hitech.cplire.ru; Tel.: +7-495-6293418

<sup>†</sup> One part of this paper is an extended version of abstract published in online Proceedings of the International Symposium on Space Terahertz Technology, ISSTT-2017, Cologne, Germany, 13–15 March 2017.

**Featured Application:** The results described in this paper will be used to develop low-noise receiving systems for ground-based radio telescopes and future space missions.



**Citation:** Rudakov, K.I.; Khudchenko, A.V.; Filippenko, L.V.; Paramonov, M.E.; Hesper, R.; da Costa Lima, D.A.R.; Baryshev, A.M.; Koshelets, V.P. THz Range Low-Noise SIS Receivers for Space and Ground-Based Radio Astronomy. *Appl. Sci.* **2021**, *11*, 10087. <https://doi.org/10.3390/app112110087>

Academic Editor: Ci-Ling Pan

Received: 20 September 2021

Accepted: 26 October 2021

Published: 28 October 2021

**Publisher's Note:** MDPI stays neutral with regard to jurisdictional claims in published maps and institutional affiliations.



**Copyright:** © 2021 by the authors. Licensee MDPI, Basel, Switzerland. This article is an open access article distributed under the terms and conditions of the Creative Commons Attribution (CC BY) license (<https://creativecommons.org/licenses/by/4.0/>).

**Abstract:** We report on research in the field of low-noise receiving systems in the sub-terahertz (THz) range, carried out in recent years, aimed at developing receivers with quantum sensitivity for implementation in space and ground-based radio telescopes. Superconductor-Insulator-Superconductor (SIS) mixers based on high-quality tunnel junctions are the key elements of the most sensitive sub-THz heterodyne receivers. Motivations and physical background for technology improvement and optimization, as well as fabrication details, are described. This article presents the results of the SIS receiver developments for the 211–275 GHz and 790–950 GHz frequency ranges with a noise temperature in the double sideband (DSB) mode of approximately 20 K and 200 K, respectively. These designs and achievements are implemented in the development of the receiving systems for the Russian Space Agency mission “Millimetron”, and for the ground-based APEX (Atacama Pathfinder EXperiment) telescope.

**Keywords:** radio astronomy; niobium-based high-quality tunnel junctions; low-noise SIS receivers; THz range quantum-limited mixers

## 1. Introduction

The development of ultra-sensitive terahertz (THz) receivers is nowadays one of the most intensively and successfully explored areas of superconducting electronics [1,2]. Superconducting elements offer an extremely high characteristic frequency and very strong nonlinearity. This makes it possible to develop systems for receiving a THz signal with unique parameters unattainable for devices based on other principles. Many applications require a spectral resolution of  $\Delta f/f \sim 10^6$ ; this can only be achieved with heterodyne receiving systems. The heterodyne mixer down-converts the weak input signal of interest to a lower intermediate frequency (IF) without loss of phase; the spectrum of IF signal is the same as the input one, but is shifted down in frequency by LO frequency. A heterodyne receiver is sensitive to two input frequency bands, spaced on either side of the LO frequency by the IF—double sideband (DSB) mode. The signal of interest usually appears in only one of these bands (signal band); unwanted noise and spurious radiation received in the other sideband (image) can be suppressed by eliminating image frequencies—single sideband (SSB) mode.

Currently, the most developed are two types of superconducting mixers: SIS mixers [1–6] for frequencies from 0.2 to 1.2 THz and hot-electron bolometer (HEB) mixers [7–11] for frequencies of 1–5 THz. Both types of mixers are mainly used in radio astronomy, where low receiver noise is a critical issue. The parameters requested by astronomers can only be realized using superconducting mixing elements with extremely low intrinsic noise, determined by the nature of the elements and cryogenic operating temperature.

The mixers based on SIS tunnel junctions are the most developed input devices for heterodyne receivers at frequencies  $f$  from 0.1 to approximately 1.2 THz. The sharp non-linearity in the tunneling current of the SIS junction is used for the mixer operation; this nonlinearity results from a single-electron tunneling process between two superconductors separated by a very thin oxide insulating layer. To describe this tunneling current under the influence of a local oscillator (LO) signal a quantum-mechanical description is required [3,4]. This process is known as photon assisted tunneling [4], as a result quasi-particle steps appear in the SIS current-voltage characteristic (IVC). Intrinsically the SIS mixers can exhibit conversion gain; important advantages of such mixers are a low LO power requirement and very low intrinsic noise [1–5]. Mixer noise temperature (DSB) is limited by the quantum value  $hf/(2k_B)$  [6], where  $h$  and  $k_B$  are the Planck and Boltzmann constants, respectively. The SIS mixers were already successfully used both for space missions like Hershel HIFI [12] and for the ground-based telescopes (including the largest ALMA multi-element interferometer [13], the European NOEMA interferometer [14], and the APEX telescope [15]).

The development of superconducting electronics makes it possible to create a superconducting integrated receiver (SIR) [16], which combines all receiver components in one microcircuit: a planar antenna, an SIS mixer, a superconducting local oscillator based on a flux-flow oscillator (FFO), and a SIS harmonic mixer for FFO phase locking. SIR sensitivity and spectral resolution were demonstrated by atmospheric limb sounding on board a high-altitude balloon [17]. SIR has been successfully implemented in the laboratory for detailed spectral measurements of THz radiation emitted from the BSCCO mesa at frequencies up to 750 GHz [18], as well as for recording sub-THz radiation of the human body under physiological stress [19].

The Russian space observatory “Millimetron” [20] with a 10-m coolable telescope, a successor of the Russian ground-space interferometer “Radioastron”, is designed to study different objects in the universe, including black holes, at sub-THz and THz frequencies. As an event horizon of a black hole is very compact, an extremely high angular resolution is required to observe details of these objects. Such a resolution will be provided by the “Millimetron” orbit configuration in combination with ground-based telescopes [21]; the observatory will be located in the vicinity of the Lagrange point L2, at 1.5 million km from Earth. For the Space-Earth interferometer, single sideband 211–275 GHz receivers sensitive for both side-bands (2SB) with a noise temperature below 50 K are required. In this paper, the results of the development of a prototype of the DSB SIS waveguide receiver with suitable parameters are presented.

The CHAMP+ heterodyne array [22] was installed on the APEX telescope and tested in 2006 [23]. The instrument consists of two separate sub-arrays of 7-pixels each; the pixels are placed in a hexagonal configuration. The input frequency ranges of two sub-arrays were chosen in accordance with the atmospheric transparency windows: 600–720 GHz and 790–950 GHz for low and high band, correspondingly. The low-frequency sub-array utilized state-of-the-art SIS mixers that were initially developed for the ALMA Band 9 receivers [24]. For high frequency mixers, only a preliminary design was made without performance optimization. Over the last decade, the technology of sub-THz SIS mixers has been greatly improved; a new generation of high-frequency range CHAMP+ detectors was developed. This article describes the characteristics of the optimized high-frequency CHAMP+ mixers and compares them with previous results.

## 2. Materials and Methods

### 2.1. Nb/AlO<sub>x</sub>/Nb and Nb/AlN/NbN SIS Mixers

The implementation of quantum-limited characteristics requires SIS tunnel junctions with an extremely low leakage current below a gap voltage  $V_g$  and a minimum spreading of the energy gap  $\delta V_g$ . This is especially important for low-frequency devices ( $f < 300$  GHz), since the  $\delta V_g$  should be much smaller than the quasiparticle step size  $hf/e$ , and the leakage current at a bias voltage around  $V_g - hf/2e$  (in the middle of this step) determines the noise of the mixer. The well-developed technology of the Nb–AlO<sub>x</sub>–Nb tunnel junctions is based on the fact that a very thin Al layer can completely cover the base Nb electrode [25–28], effectively planarizing the column-like microstructure of the Nb film [27]. This Al layer is subsequently oxidized and the top Nb electrode is deposited on the oxidized layer to form a so-called three-layer structure.

The selective niobium etching and anodization process (SNEAP) [26] was used to fabricate the SIS tunnel junctions from the Nb/Al–AlO<sub>x</sub>/Nb three-layer structure circuits [28–30] on 24 × 24 mm quartz substrates. To prevent etching of the substrate at the junction definition process and to simplify photolithography on a transparent substrate, a “monitor” Nb layer with a thickness of approximately 100 nm was applied to the substrate using DC magnetron sputtering. The next step is the deposition of a three-layer structure, which was carried out using DC magnetron sputtering in one vacuum cycle. First, a 200 nm thick lower niobium layer is deposited together with a 5 nm thick barrier aluminum layer. After that, the aluminum surface is oxidized in an atmosphere of pure oxygen, and a layer of upper Nb is deposited with a thickness of 100 nm. The geometry of the base electrode is formed by lift-off.

SIS junctions are formed by reactive ion etching (RIE) in CF<sub>4</sub>; the top layer of the Nb three-layer structure is removed in accordance with a mask from the photoresist defining the geometry of the junction. The AlO<sub>x</sub> barrier layer acts as a stop layer, preventing further etching of the structure. After RIE, light anodization is carried out up to 10 V using the same photoresist mask, then, an insulating SiO<sub>2</sub> layer with a typical thickness of 250 nm is deposited using RF magnetron sputtering. The opening of the contacts to the SIS junctions is carried out by lift-off. The upper electrode is also formed by the lift-off process from the deposited niobium layer with a thickness of 350–400 nm. The gold contact pads of the base and top electrodes are formed in a similar manner.

Usually, the well-pronounced knee-like feature arises on the IVC at voltages slightly higher than  $V_g$ . This feature is due to the presence of the aluminum layer near the tunnel barrier; the IVC of the Nb/Al–AlO<sub>x</sub>/Nb (S–S′/I/S) tunnel junction depends on the quasiparticle density of states in the S′ layer (Al). This density of states for the Nb/Al bilayers was calculated using the microscopic proximity effect model [31]. The model assumes a short electron mean-free path (dirty limit conditions) in both S (Nb) and S′ (Al) materials. Experimentally, the dependence of this effect on the parameters of the tunnel structure was investigated in [28]. The presence of the knee structure results in the negative differential resistance on the quasiparticle steps that in turn leads to the mixer instability and nonlinear operation at some frequencies.

It was demonstrated that the knee structure can be completely suppressed by introducing an additional Al layer in the base electrode. The current-voltage characteristic (IVC) of an Nb–Al–Nb/Al–AlO<sub>x</sub>/Nb SIS mixing element (area of approximately 1 μm<sup>2</sup>) with an additional Al layer in the bottom electrode, measured in the voltage-bias mode, is shown in Figure 1; the SIS junction critical current is suppressed by a magnetic field. The normal resistance of the SIS junction is  $R_n = 22 \Omega$ ; the quality parameter characterized by the ratio of the resistances under and above the gap  $R_{sg}/R_n = 39$ ; the gap voltage  $V_g = 2.8$  mV, and the energy gap spreading  $\delta V$  is approximately 0.1 mV.

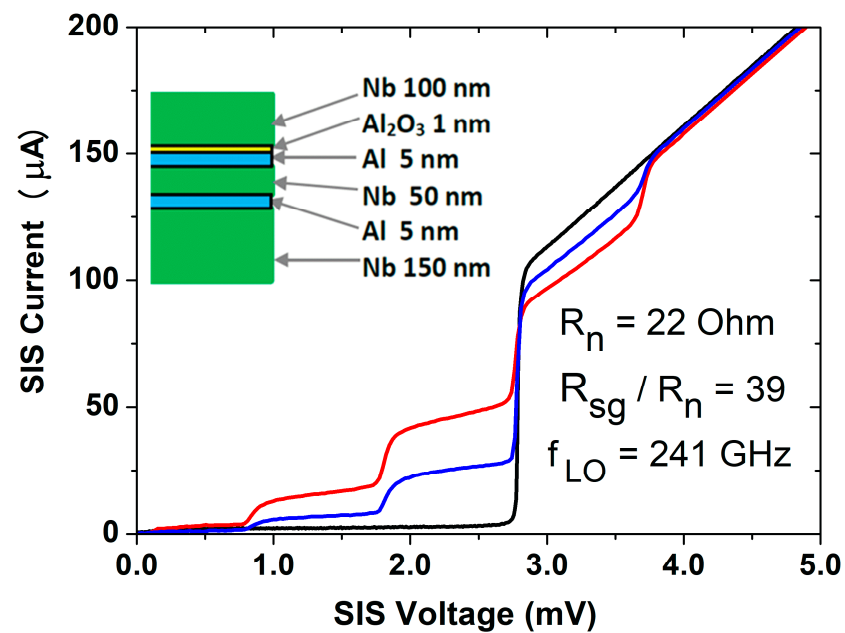


**Figure 1.** IVC of the Nb-Al-Nb/Al-AlO<sub>x</sub>/Nb mixer element fabricated on quartz substrate (area of tunnel junction  $A = 1 \mu\text{m}^2$ ,  $V_g = 2.8 \text{ mV}$ ,  $R_n A = 22 \Omega \mu\text{m}^2$ ); the Josephson supercurrent is suppressed by the magnetic field (black line). The IVCs of the SIS mixer pumped by LO at 241 GHz at two different LO powers are shown by the blue and red lines. A cross-section of the three-layer structure is presented in the inset.

To realize a quantum-limited performance of the SIS mixers at sub-THz frequencies, several important issues should be considered:

(1) For operation at sub-THz frequencies, tunnel junctions with very high tunnel barrier transparencies are required. Unfortunately, there is a limit to the increasing of the AlO<sub>x</sub> barrier transparency (current density of approximately 10–15 kA/cm<sup>2</sup>); at a higher current density, abrupt degradation of the junction's quality takes place. This problem was overcome by the development of Nb/Al-AlN/Nb tunnel junctions that demonstrate reasonably good  $R_{sg}/R_n > 10$  at very high current densities of up to 100 kA/cm<sup>2</sup> [32–35]. The procedure for fabrication of the Nb/AlN/Nb junction follows the well-known recipe for Nb/AlO<sub>x</sub>/Nb circuits that was described above; the only difference is the replacement of the oxidation with the nitridization process. To achieve a good matching between such high current density junctions and the antenna, submicron SIS junctions are required;

(2) The operating frequency of the Nb SIS receivers is constrained by the gap frequency of Nb (approximately 700 GHz). The possible solution for this problem may be found in the fabrication and utilization of the devices with microstrip lines based on compounds of Nb with the higher gap frequencies, particularly NbTiN; the top electrode of the line is usually made from normal metal to avoid SIS junction overheating [36–38]. We developed an SIS mixer based on high critical current density Nb/AlN/NbN tunnel junctions embedded in a microstrip line consisting of a 320 nm NbTiN lower electrode (ground plane) and a 500 nm Al upper electrode [39]. The microstrip electrodes are separated by a 250 nm thick SiO<sub>2</sub> insulating layer. The SIS junction is placed on the NbTiN film and the top NbN layer is in contact with the upper Al electrode (see inset in Figure 2). A detailed procedure for making the circuit is described in [39].

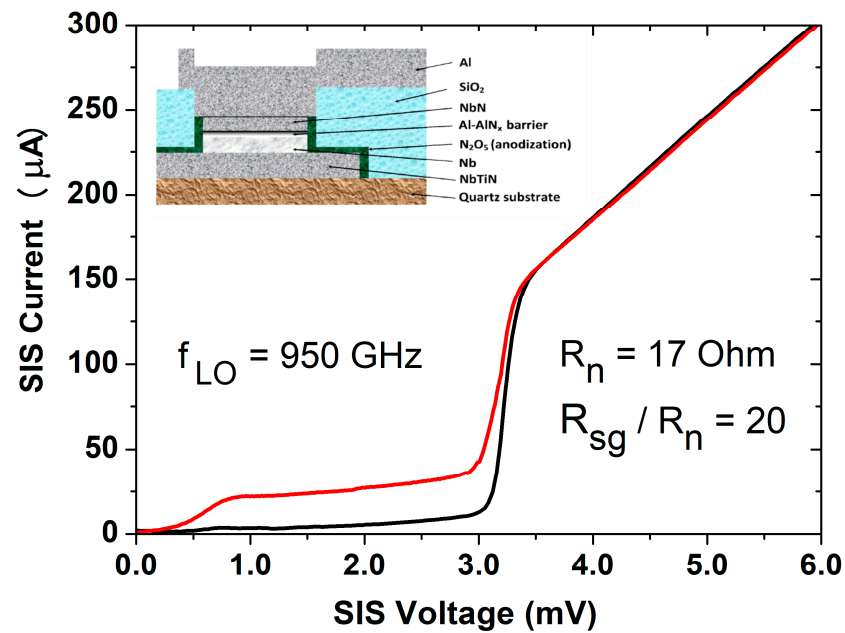


**Figure 2.** IVC of the Nb/AlN/NbN mixer element inserted in the NbTiN/Al stripline, fabricated on quartz substrate for APEX telescope (area of tunnel junction  $A = 0.5 \mu\text{m}^2$ ,  $V_g = 3.22 \text{ mV}$ ,  $R_n S = 8.5 \Omega \mu\text{m}^2$ ,  $J_g$  of approximately  $30 \text{ kA/cm}^2$ ); the Josephson supercurrent is suppressed by the magnetic field (black line). IVC of the SIS mixer pumped by a CW LO source delivering approximately  $0.5 \mu\text{W}$  of power to the SIS junction at  $950 \text{ GHz}$  is shown by the red line. A cross-section of the mixer element incorporated in a NbTiN/Al microstrip line is presented in the inset.

(3) The frequency of  $950 \text{ GHz}$  corresponds to a quasiparticle step size of  $3.9 \text{ mV}$ , which exceeds the  $V_g$  of conventional SIS junctions with Nb electrodes ( $V_g < 2.8 \text{ mV}$  for Nb/AlN/Nb junctions with high current density). Further, the quasiparticle step from the negative IVC branch suppresses the positive step and decreases the voltage range available for the SIS mixer biasing, considering the presence of the unsuppressed Shapiro step feature [40] right on the quasiparticle step. The use of an AlN tunnel barrier in combination with an NbN superconducting top electrode provides a significant improvement in the performance of the SIS THz mixer since much higher gap voltages can be realized. To investigate this idea, we developed the Nb/AlN/NbN tunnel junction [30,41]. The NbN film was deposited by DC-reactive magnetron sputtering at ambient temperature, with  $1.8 \text{ W/cm}^2$  power density using an Ar + 9%  $\text{N}_2$  gas mixture. Otherwise, the fabrication procedure was the same as for Nb/AlN/Nb junctions [30,41]. The IV characteristic of such junctions fabricated on Si substrates demonstrated quality factor  $R_{sg}/R_n > 30$  at the current density up to  $10 \text{ kA/cm}^2$  and a gap voltage as high as  $3.7 \text{ mV}$  [41,42]. For the Nb/AlN/NbN junctions with  $0.5 \mu\text{m}^2$  area fabricated on an Si substrate, a gap voltage  $V_g = 3.5 \text{ mV}$  was measured. In contrast, the Nb/AlN/NbN junctions with thin ( $100 \text{ nm}$ ) Nb electrodes fabricated on the NbTiN film have  $V_g = 3.22 \text{ mV}$  and quality  $R_{sg}/R_n = 20$  for  $R_n A = 8.5 \Omega \cdot \mu\text{m}^2$  (current density is of approximately  $30 \text{ kA/cm}^2$ ), see Figure 2.

To design a low-noise THz-mixer, the capacitance of an SIS junction should be tuned out by specially-designed inductive elements; for that, the junction capacitance should be determined with high accuracy, i.e., the main parameters of the tunnel barrier (average barrier height  $\phi$  and thickness  $d$ ) must be evaluated. We determined the tunnel barrier thickness and its average height from the IVCs at high voltages [43] as proposed by Simmons [44] and as generalized by Brinkman for tunnel junctions in the limit of low bias voltages [45]. The main parameters of the tunneling barrier of the Nb/AlO<sub>x</sub>/Nb and Nb/AlN/Nb junctions are estimated in a wide range of current densities, see Figure 3. A decrease in the height of the tunnel barrier of the junction with the AlN barrier by  $0.3 \text{ eV}$  in comparison with the oxide junction makes it possible to realize SIS junctions with a current

density of more than  $15 \text{ kA/cm}^2$  with an insulating layer thickness of approximately  $1 \text{ nm}$  that is allowable technologically, which makes it possible to obtain a quality parameter  $R_{sq}/R_n$  as high as 25, even for high current density ( $R_n A < 10 \Omega \cdot \mu\text{m}^2$ ).

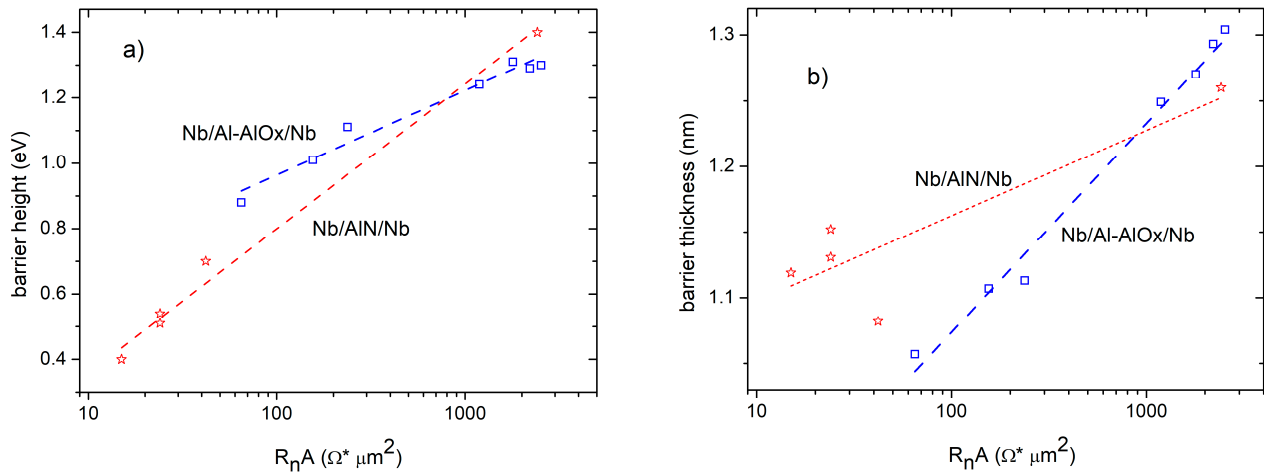


**Figure 3.** Dependence of the tunnel barrier parameters on resistivity  $R_n A$ : (a) barrier height  $\phi$ ; (b) barrier thickness  $d$ . Data for the Nb/AIO<sub>x</sub>/Nb junctions are shown by squares and for the Nb/AlN/Nb junctions by asterisks; the dotted and dashed lines are linear approximations for appropriate data.

## 2.2. Mixer and Mixer Block Designs

In the design of the mixer block for the frequency range 211–275 GHz, we follow a successful modular construction approach developed for the ALMA Band 9 receiver [24]. The mixer block (see Figure 4) consists of a few separate elements: (1) an input horn; (2) a central part with the waveguide; (3) a back piece (BP) unit where the mixer chip is installed; and (4) a magnet block unit with two magnet pins to suppress the Josephson critical current of the SIS mixer. The receiving chip (width  $150 \mu\text{m}$ ) is located in a rectangular  $1000 \times 500 \mu\text{m}$  waveguide at a distance of  $230 \mu\text{m}$  from the back short in the waveguide, orthogonal to the propagation direction (Figure 5). The Nb/AIO<sub>x</sub>/Nb SIS junction is placed into a planar Nb/SiO<sub>2</sub>/Nb tuning structure made on a  $125 \mu\text{m}$  thick quartz substrate. To prevent leakage of the high frequency input signal through this dielectrically filled waveguide, blocking low-pass filters were used.

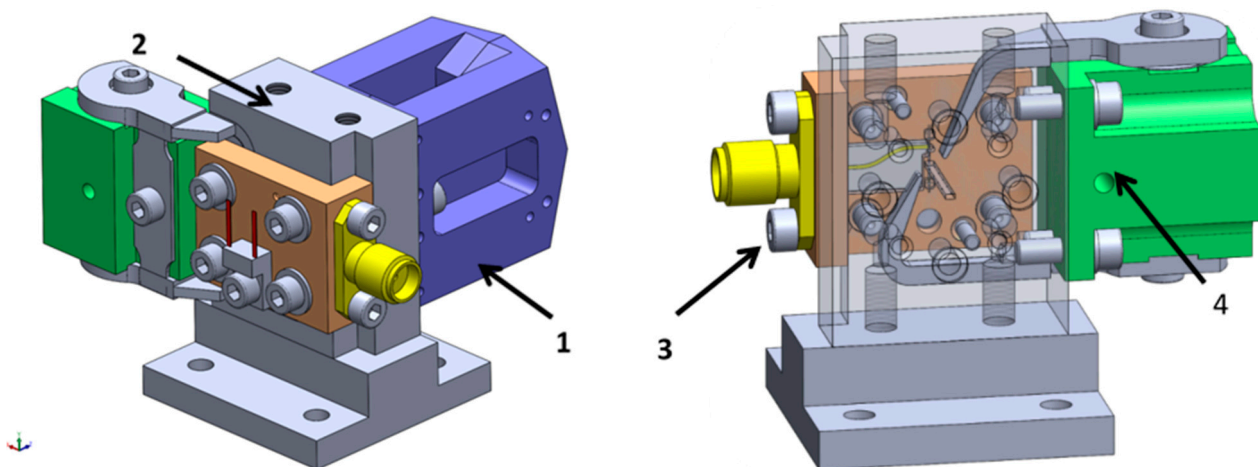


**Figure 4.** A 3D model of the mixer block for the frequency range 211–275 GHz; all main parts are shown: (1) input horn, (2) central part with the waveguide, (3) back piece with mixer chip, (4) magnet block unit.

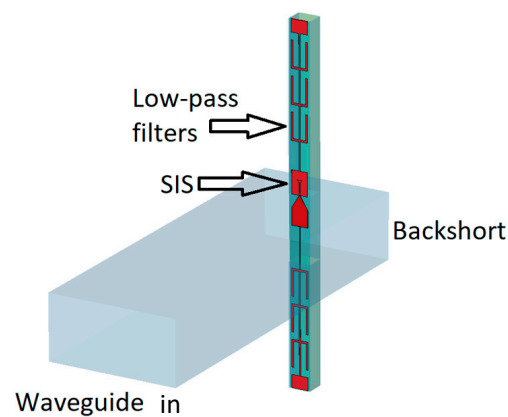


**Figure 5.** A 3D model for a double-side mixer placed inside a waveguide channel. The input horn is placed in the front side of the waveguide mixer block (Waveguide in), and the back short position is marked in a back view.

To achieve a good SIS mixer performance, the tunnel junction should be matched properly with the input waveguide impedance at high frequencies and with a 50 Ohm amplifier impedance in the whole IF frequency band. To match the waveguide impedance of approximately 400 Ohm and the high frequency SIS impedance, a waveguide probe and a tuning structure were used. A combination of the coplanar (CPW) and microstrip (MSL) lines was used to tune out the intrinsic SIS capacitance and to provide the matching of the resulting SIS impedance to the waveguide at high frequencies (see Figure 6). This approach allowed us to make the tuning structures more compact. As the wavelengths in the tuning lines in the range of IF are much larger than the dimensions of the structure, the tuning microstrip lines add some capacitance to the sample impedance on the IF. To adjust the output impedance of the receiver, a matching circuit should be implemented at the mixer output. In this work, we used a PCB with a 50 Ohm line without any additional tuning elements (see Figure 7).

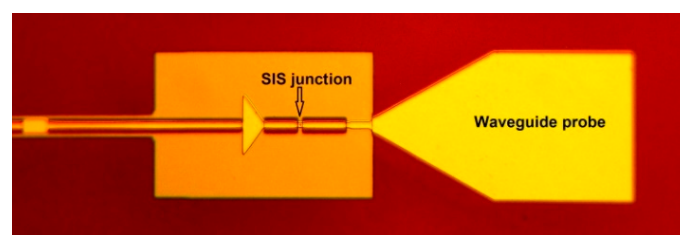


**Figure 6.** Photo of the SIS mixer structure for the frequency range 211–275 GHz. The SIS element is inserted in the planar structure formed by segments of coplanar and microstrip Nb-SiO<sub>2</sub>-Nb lines. The waveguide probe is shown on the right.

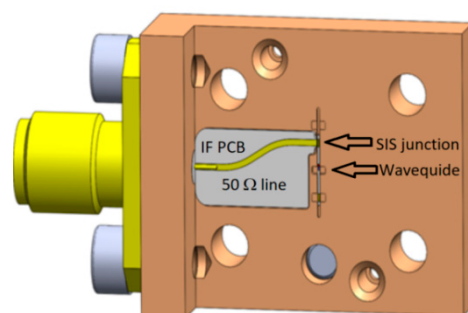


**Figure 7.** A 3D model of the back piece. A PCB plate, the SIS mixer element and waveguide are depicted.

To make a wideband receiver for the 790–950 GHz frequency range for CHAMP+, we used twin SIS junctions [46,47] (each with an area of  $0.5 \mu\text{m}^2$ , see Figure 8), coupled by a waveguide probe to the E-field of a rectangular waveguide of  $300 \times 75 \mu\text{m}$ . The SIS mixer [48,49] was based on high critical current density Nb/AlN/NbN tunnel junctions included in the NbTiN-Al microstrip line [39]. The microstrip electrodes (320 nm thick bottom NbTiN electrode and a 500 nm thick top electrode made of Al) were separated by a 250 nm  $\text{SiO}_2$  insulator. The detailed procedure for making the circuit is described in the previous subsection.

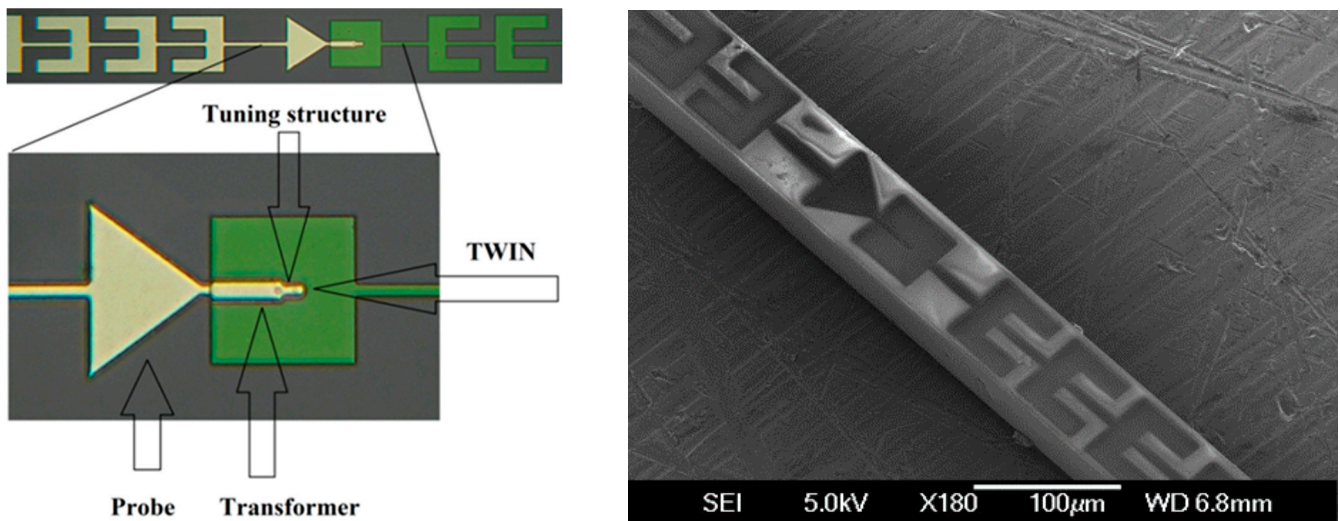


**Figure 8.** Layout (left) and SEM photo (right) of the CHAMP+ high band SIS mixer. The central part of the chip (including SIS twin junction, transformer, and probe) is magnified.

Due to the high current density of the AlN barrier, a lower  $R_n$  value is realized, which gives a higher  $1/R_n C$  ratio for junctions (with  $C$ -junction capacitance), providing a wider reception bandwidth. A twin mixer circuit was formed by two SIS junctions with  $6.5 \mu\text{m}$  junction spacing, embedded in a  $4.5 \mu\text{m}$  wide microstrip line, which is connected to the antenna by a  $7 \times 27 \mu\text{m}$  impedance transformer [44] designed to match the high current density junctions to the waveguide probe (see Figure 8).

### 3. Experimental Results

#### 3.1. 211–275 GHz SIS-Mixer Measurements

To evaluate a wideband radiation matching of the SIS mixer at sub-THz frequencies, the Michelson Fourier transform spectrometer (FTS) technique was used [43,44]. A wideband sub-THz glow bar source (1500 K black body) was matched with the FTS, which was loaded by the SIS mixer as a detector. The mixer was voltage biased at 2.5 mV; a direct current response was measured versus a mirror position. These data were Fourier-transformed into a mixer response on the frequency. The experimental data demonstrate a good agreement with the results of numerical simulations [48,49].

The DSB mixer noise temperature was determined by the standard Y-factor measurement method; an absorber at room temperature (295 K) was used as a “hot” load, and an absorber cooled by liquid nitrogen (78 K) was used as a “cold” load [48,49]. Figure 9 shows the SIS receiver output versus the bias voltage measured for 241 GHz LO at 6.5 GHz IF (60 MHz IF filter bandwidth). The Y-factor was determined by subtracting the responses measured for hot and cold loads. The value of the Y-factor at the best point exceeds 5.0 dB, which corresponds to a receiver noise temperature of approximately 22 K. The values of the noise temperature  $T_n$  were obtained without any corrections for losses in the beam splitter and the cryostat window [49]; they were only twice the value of  $hf/k_B$  in the frequency range from 240 to 275 GHz (see Figure 10); the obtained values meet the technical requirements



for the 211–275 GHz receiver of the Millimetron space radio telescope. It should be noted that the receiver linearity was confirmed by direct measurements at most frequencies in the tuning range, except for two points around 260 GHz; these points were excluded from Figure 10.

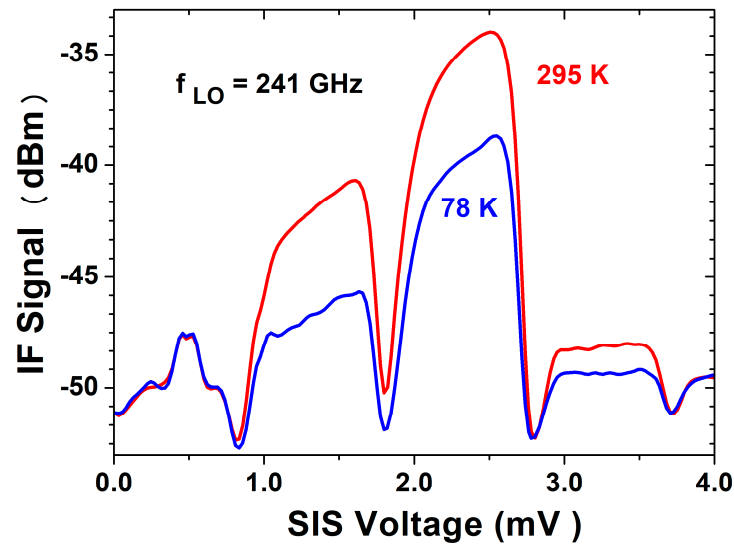


Figure 9. The output signal of the SIS receiver at intermediate frequency (IF) 6.5 GHz on the SIS bias voltage, measured for the cold and hot input loads (78 K—blue curve and 295 K—red curve, correspondingly) at the local-oscillator frequency 241 GHz.

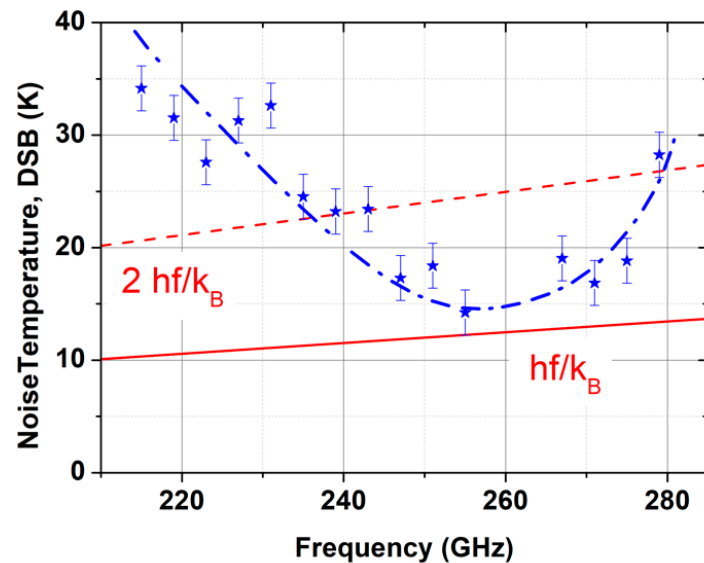


Figure 10. DSB receiver noise temperature of the SIS receiver on the local oscillator (LO) frequency; the experimental data are presented without any corrections for losses in the input optic elements. Measurement uncertainty is approximately 2 K, shown by error bars. The dash-dotted line is given as a guide for the eyes.

A detailed description of mixer noise breakdown was discussed in Ref. [49]; the estimates of the contributions of the device components can be listed as follows: (a) 6 micron mylar beam splitter—0.6 K; (b) receiver input window—0.5 K; (c) IF circuit (which is a combination of a Pamtech 4–12 GHz cryogenic isolator and a cryogenic amplifier)—6 K. Note that the quantum limit for the DSB SIS mixer element is  $hf/2k_B$  [6]; which corresponds to 5.8 K at 250 GHz. The receiver stability at a 241.2 GHz LO frequency was evaluated by recording the receiver output vs. time at the same operating conditions as for noise

temperature measurements. The hot load was presented in the form of the receiver. A 60 MHz bandpass filter was used to limit the signal bandwidth. An Allan time up to 10 s was registered [49] determined by the stability of the set-up components and is a typical value for all SIS mixers evaluated in this setting.

### 3.2. High Band (790–950 GHz) Mixers

The SIS mixers for the waveguide receiver with an operation frequency up to 950 GHz were developed and tested [49–51]; these mixers are based on Nb/AlN/NbN twin tunnel junctions incorporated in a NbTiN/Al microstrip line and are intended for the Chinese radio observatory at Dome A, Antarctic, for Champ II+ (APEX observatory at Atacama site in Chile) and Brazilian LLAMA located in the Andes. The above technology makes it possible to achieve a junction current density of up to 30 kA/cm<sup>2</sup>; providing a figure of merit (the ratio of the resistance of the sub-gap to normal) above 20. Using the twin SIS junction design, we have achieved a wide receiver operating range (675 to 950 GHz) and quite good noise temperature in this frequency range, as shown in Figure 11.

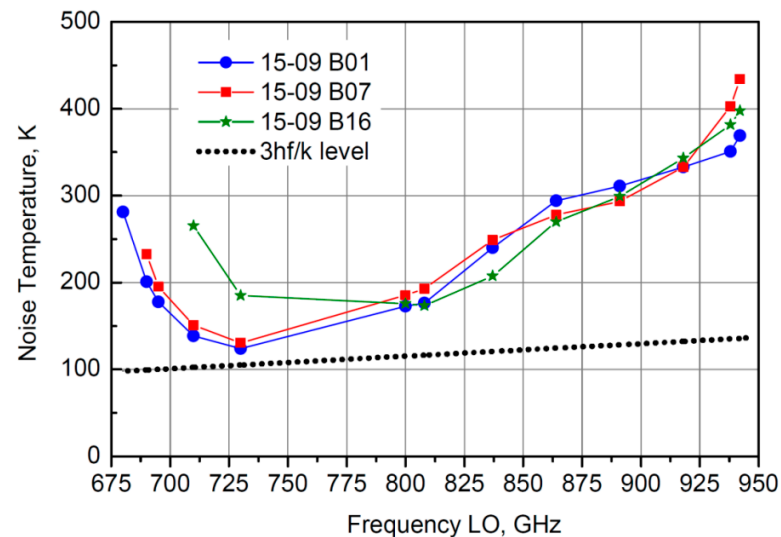


**Figure 11.** DSB noise temperature for three SIS mixers as a function of frequency; noise temperature was corrected for losses in the input window and beam splitter. The dotted line shows the noise temperature, which corresponds to  $3hf/k_B$ .

The original CHAMP + high-frequency mixers used Nb/AlO<sub>x</sub>/Nb SIS technology; the high-frequency mixers were based on twin SIS junctions, as opposed to the single-junction design for the low frequency range; the twin junction circuit was inserted into a microstrip line with an NbTiN bottom and an aluminum top wire [22], similar to HIFI band 3 mixers [36]. The photos of the high band (790–950 GHz) array of 7-pixels, placed in a hexagonal configuration, are presented in Figure 12. Since the one-off design was created without further iteration, the performance of previous mixers was not optimized, leaving room for improvement. The noise temperature of the original mixers, measured before being installed in the receiver cryostat [46], is shown in Figure 13 by blue curves. This is corrected for noise caused by input window loss and beam splitter for LO injection. The data does not cover the entire range due to the limited range of the laboratory LO (based on BWO) available at the time. These characteristics were confirmed by recent laboratory measurements of the original center pixel mixer after it was removed from the telescope (green curve in Figure 13) [51]. Generally speaking, the noise temperature of the original mixers ranges from 300–400 K at low frequencies to double the value at high frequencies.

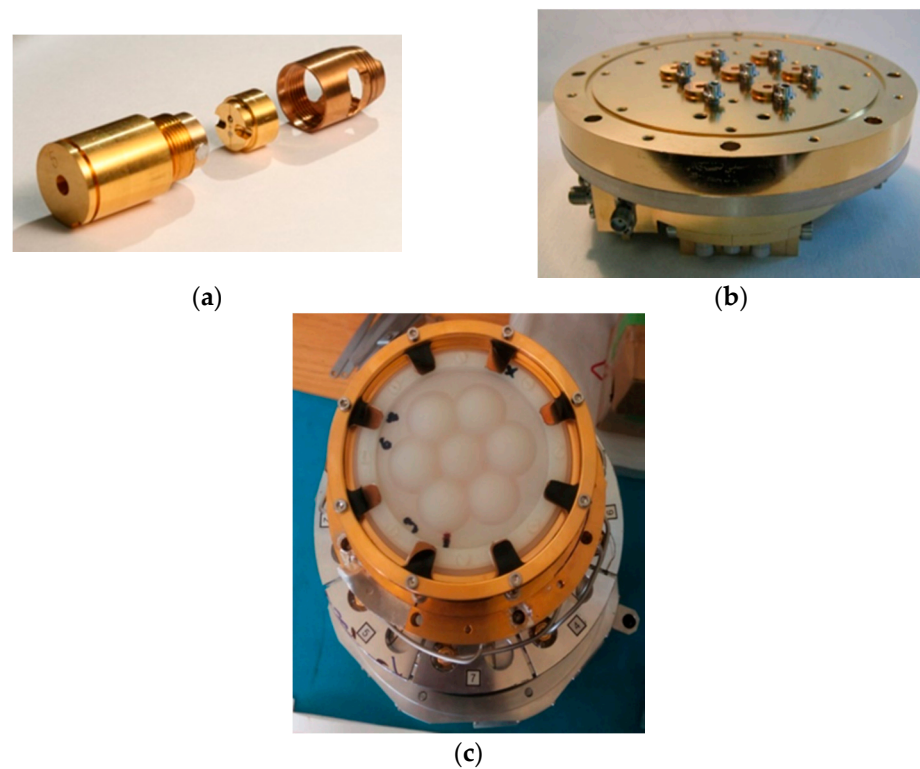


**Figure 12.** 7-pixel array for high band (790–950 GHz) receiver CHAMP+ at radio telescope APEX (Atacama Pathfinder EXperiment): (a) Photo of the pixel mixer block elements, (b) 7-pixel mixer array with open horns, (c) Lens array at the top of the cartridge body.

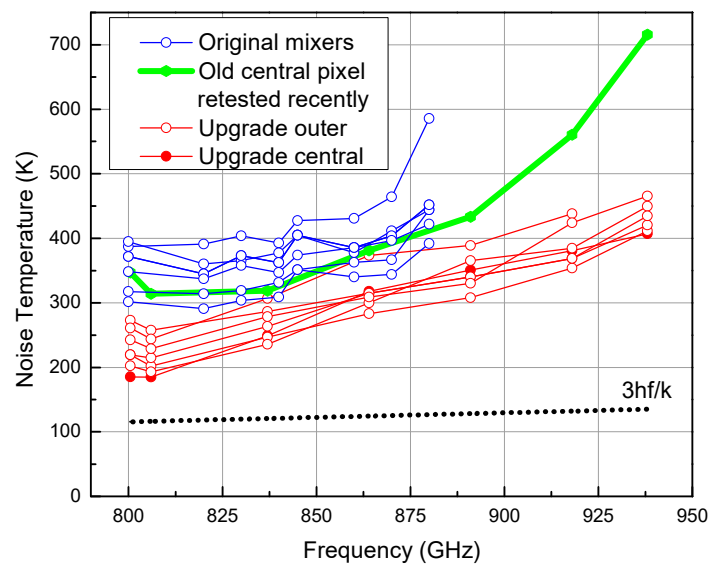


**Figure 13.** DSB mixer noise temperature for the entire 4–12 GHz IF band vs. LO frequency. The noise temperature is corrected for approximately 10% insertion loss of a beam splitter and the hot LO (300 K) contribution. The old mixers' performances (blue curves), including the additional recent verification for the central pixel (green curve), are compared here with the results for the new mixers (red curves) [51].

To upgrade high frequency receivers, we have developed mixers based on twin Nb/AlN/NbN SIS junctions embedded in the NbTiN/Al line [38,49–51]. This technology allowed us to significantly improve the performance of the 7-pixel array for the CHAMP+ instrument, mounted on the APEX (Atacama Pathfinder EXperiment) telescope, input

frequency range 790–950 GHz, IF range 4–12 GHz. All upgraded mixers used the second minimum critical current when suppressed by the magnetic field; the DSB noise temperature for upgraded mixers is shown in Figure 13 with red curves [51]. From the data presented in Figure 13, we can conclude that the modernization of the mixers should improve the sensitivity of the CHAMP + high frequency range by 1.3–1.5 times [51]. In the case of good weather conditions, given an atmosphere transparency of approximately 50% [52], the mapping speed will be improved by approximately 40%.

In addition to the integrated IF data in Figure 13, we measured [51] the IF spectra for all LO points; the best IF noise temperature in the 4–12 GHz range on LO frequency is shown in Figure 14. As expected, it is lower than the integrated results, although the consistency of the curves does not change—the mixer with the lowest noise temperature in Figure 13 remains the best and in Figure 14 [51]. The data in Figure 14 demonstrate the receiver performance at typical spectral lines radio astronomy observations.

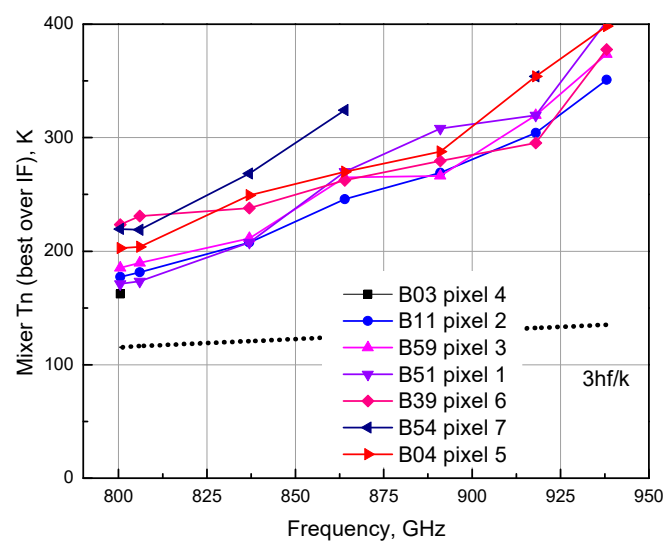


**Figure 14.** The best noise temperature over the IF band as a function of LO frequency. The data are corrected for the beam splitter the same as in Figure 13.

#### 4. Conclusions

We designed, fabricated, and tested a DSB SIS mixer for the frequency range of 211–275 GHz. The uncorrected receiver noise temperature of approximately  $16.5 \pm 2$  K was measured at frequency 255 GHz, which exceeds the quantum value  $hf/k_B$  only slightly. This mixer is developed as a prototype for the Millimetron Space mission or future astronomy instruments, and it can be used for novel ground-based radio telescopes (Suffa [53], LLAMA [54]).

To upgrade the high-frequency receivers, we have employed Nb/AlN/NbN mixers incorporated in an NbTiN/Al line. The presented mixer technology in comparison with Nb/AlO<sub>x</sub>/Nb mixers looks quite promising: (1) a higher  $V_g$  value provides a 0.7 mV wider quasiparticle step for high frequencies; (2) high current density allows for a very broadband mixer; (3) heating of the SIS junctions is not critical for the operation of the mixer. SIS mixers designed to upgrade the CHAMP + high frequency array (790–950 GHz) on the APEX telescope exhibit DSB noise temperatures of 210 to 400 K. This improves sensitivity by up to 40% (i.e., almost a factor of 2 in observation time).

**Author Contributions:** Conceptualization, A.M.B., V.P.K.; methodology, K.I.R., A.V.K., R.H., L.V.F. and M.E.P.; mixer block design R.H., K.I.R., A.V.K. and A.M.B.; SIS circuit fabrication, L.V.F.; Tunnel barrier measurements, M.E.P. electromagnetic simulations were performed by, K.I.R., A.V.K. and A.M.B.; experiments were performed by, K.I.R., A.V.K., M.E.P., R.H., D.A.R.d.C.L. and A.M.B.; data analysis, K.I.R., A.V.K., M.E.P., A.M.B. and V.P.K.; writing and editing, K.I.R., A.V.K., and V.P.K.;

funding acquisition, A.M.B. and V.P.K. All authors have read and agreed to the published version of the manuscript.

**Funding:** The work was supported by the Russian Foundation for Basic Research (grant No. 19-52-80023). The development and fabrication of the 211–275 GHz SIS mixers was supported by the RSF grant 19-19-00618. The equipment of USU “Cryointegral” was used to carry out the research; USU is supported by a grant from the Ministry of Science and Higher Education of the Russian Federation, agreement No. 075-15-2021-667. The work is also supported by Netherlands Academy of science (NWO) grant “NWO-FAPESP Advanced Instrumentation for Astronomy” number 629.004.00.

**Conflicts of Interest:** The authors declare no conflict of interest.

## References

1. Zmuidzinas, J.; Richards, P.L. Superconducting detectors and mixers for millimeter and submillimeter astrophysics. *Proc. IEEE* **2004**, *92*, 1597–1616. [CrossRef]
2. Sizov, F.; Rogalski, A. THz detectors. *Prog. Quantum Electron.* **2010**, *34*, 278–347. [CrossRef]
3. Tucker, J.R. Quantum Limited Detection in Tunnel Junction Mixers. *IEEE J. Quantum Electron.* **1979**, *15*, 1234–1258. [CrossRef]
4. Tucker, J.R.; Feldman, M.J. Quantum Detection at millimeter wavelengths. *Rev. Mod. Phys.* **1985**, *57*, 1055–1113. [CrossRef]
5. Richards, P.L.; Shen, T.M.; Harris, R.E.; Lloyd, F.L. Quasiparticle heterodyne mixing in SIS tunnel junctions. *Appl. Phys. Lett.* **1979**, *34*, 345–347. [CrossRef]
6. Kerr, A.R.; Feldman, M.J.; Pan, S.-K. Receive Noise Temperature, the Quantum Noise Limit, and the Role of the Zero-Point Fluctuations. In Proceedings of the Eighth International Symposium on Space Terahertz Technology, Cambridge, MA, USA, 25–27 March 1997.
7. Semenov, A.D.; Gol'tsman, G.N.; Sobolewski, R. Hot-electron effect in superconductors and its applications for radiation sensors. *Supercond. Sci. Technol.* **2002**, *15*, R1–R16. [CrossRef]
8. Shurakov, A.; Lobanov, Y.; Goltsman, G. Superconducting hot-electron bolometer: From the discovery of hot-electron phenomena to practical applications. *Supercond. Sci. Technol.* **2016**, *29*, 1–27. [CrossRef]
9. Gao, J.R.; Hovenier, J.N.; Yang, Z.Q.; Baselmans, J.J.A.; Baryshev, A.; Hajenius, M.; Klapwijk, T.M.; Adam, A.J.; Klaassen, T.O.; Williams, B.S.; et al. A terahertz heterodyne receiver based on a quantum cascade laser and a superconducting bolometer. *Appl. Phys. Lett.* **2005**, *86*, 244104. [CrossRef]
10. Cherednichenko, S.; Drakinskiy, V.; Berg, T.; Khosropanah, P.; Kollberg, E. Hot-electron bolometer terahertz mixers for the Herschel Space Observatory. *Rev. Sci. Instrum.* **2008**, *79*, 034501. [CrossRef]
11. Maezawa, H. Application of Superconducting Hot-Electron Bolometer Mixers for Terahertz-Band Astronomy. *IEICE Trans. Electron.* **2015**, *E98*, 196–206. [CrossRef]
12. De Graauw, T.; Helmich, F.P.; Phillips, T.G.; Stutzki, J.; Caux, E.; Whyborn, N.D.; Dieleman, P.; Roelfsema, P.R.; Aarts, H.; Assendorp, R.; et al. The Herschel—Heterodyne Instrument for the Far-Infrared (HIFI). *Astron. Astrophys.* **2010**, *518*, 1–7. [CrossRef]
13. Available online: <https://www.almaobservatory.org/en/about-alma-at-first-glance/how-alma-works/technologies/interferometry/> (accessed on 19 September 2021).
14. Available online: <https://www.iram-institute.org/EN/content-page-56-7-56-0-0-0.html> (accessed on 19 September 2021).
15. Available online: <https://www.eso.org/public/teles-instr/apex/> (accessed on 19 September 2021).
16. Koshelets, V.P.; Shitov, S.V. Integrated Superconducting Receivers. *Supercond. Sci. Technol.* **2000**, *13*, R53–R69. [CrossRef]
17. De Lange, G.; Birk, M.; Boersma, D.; Dercksen, J.; Dmitriev, P.; Ermakov, A.; Filippenko, L.; Golstein, H.; Hoogeveen, R.; de Jong, L.; et al. Development and characterization of the superconducting integrated receiver channel of the TELIS atmospheric sounder. *Supercond. Sci. Technol.* **2010**, *23*, 045016. [CrossRef]
18. Li, M.; Yuan, J.; Kinev, N.; Li, J.; Gross, B.; Guénon, S.; Ishii, A.; Hirata, K.; Hatano, T.; Koelle, D.; et al. Linewidth dependence of coherent terahertz emission from Bi<sub>2</sub>Sr<sub>2</sub>CaCu<sub>2</sub>O<sub>8</sub> intrinsic Josephson junction stacks in the hot-spot regime. *Phys. Rev. B* **2012**, *86*, 060505. [CrossRef]
19. Baksheeva, K.; Ozhegov, R.; Goltsman, G.; Kinev, N.; Koshelets, V.; Kochnev, A.; Betzalel, N.; Puzenko, A.; Ishai, P.; Feldman, Y. The Sub THz Emission of the Human Body under Physiological Stress. *IEEE Trans. Terahertz Sci. Technol.* **2021**, *11*, 381–388. [CrossRef]
20. Available online: <http://millimetron.ru/index.php/en/> (accessed on 19 September 2021).
21. Andrianov, A.S.; Baryshev, A.M.; Falcke, H.; Girin, I.A.; de Graauw, T.; Kostenko, V.I.; Kudriashov, V.; Ladygin, V.A.; Likhachev, S.F.; Roelofs, F.; et al. Simulations of M87 and Sgr A\* imaging with the Millimetron Space Observatory on near-Earth orbits. *Mon. Not. R. Astron. Soc.* **2021**, *500*, 4866–4877. [CrossRef]
22. Kasemann, C.; Güsten, R.; Heyminck, S.; Klein, B.; Klein, T.; Philipp, S.D.; Korn, A.; Schneider, G.; Henseler, A.; Baryshev, A.; et al. CHAMP+: A powerful array receiver for APEX. *Millim. Submillimeter Detect. Instrum. Astron. III* **2006**, 6275, 62750N. [CrossRef]
23. Güsten, R.; Booth, R.S.; Cesarsky, C.; Menten, K.M.; Agurto, C.; AnCIAUX, M.; Wyrowski, F. Ground-based and Airborne Telescopes. *Int. Soc. Opt. Photonics* **2006**, 6267, 626714.

24. Baryshev, A.M.; Hesper, R.; Mena, F.P.; Klapwijk, T.M.; van Kempen, T.A.; Hogerheijde, M.R.; Jackson, B.D.; Adema, J.; Gerlofsma, G.J.; Bekema, M.E.; et al. The ALMA Band 9 receiver. Design, construction, characterization, and first light. *Astron. Astrophys.* **2015**, *577*, A129. [[CrossRef](#)]
25. Rowell, J.M.; Gurvitch, M.; Geerk, J. Modification of tunneling barriers on Nb by a few monolayers of Al. *Phys. Rev. B* **1981**, *24*, 2278–2281. [[CrossRef](#)]
26. Gurvitch, M.; Washington, M.A.; Huggins, H.A. High quality refractory Josephson tunnel junctions utilizing thin aluminum layers. *Appl. Phys. Lett.* **1983**, *42*, 472–474. [[CrossRef](#)]
27. Imamura, T.; Shiota, T.; Hasuo, S. Fabrication of high quality Nb/AlO<sub>x</sub>-Al/Nb Josephson junctions: I—Sputtered Nb films for junction electrode. *IEEE Trans. Appl. Supercond.* **1992**, *2*, 222–227.
28. Dmitriev, P.N.; Ermakov, A.B.; Kovalenko, A.G.; Koshelets, V.P.; Iosad, N.N.; Golubov, A.A.; Kupriyanov, M.Y. Niobium tunnel junctions with multi-layered electrodes. *IEEE Trans. Appl. Supercond.* **1999**, *9*, 3970–3973. [[CrossRef](#)]
29. Filippenko, L.V.; Shitov, S.V.; Dmitriev, P.N.; Ermakov, A.B.; Koshelets, V.P.; Gao, J.R. Submillimeter superconducting integrated receivers: Fabrication and yield. *IEEE Trans. Appl. Supercond.* **2001**, *11*, 816–819. [[CrossRef](#)]
30. Dmitriev, P.N.; Lapitskaya, I.L.; Filippenko, L.V.; Ermakov, A.B.; Shitov, S.V.; Prokopenko, G.V.; Kovtonyuk, S.A.; Koshelets, V.P. High quality Nb-based tunnel junctions for high frequency and digital applications. *IEEE Trans. Appl. Supercond.* **2003**, *13*, 107–110. [[CrossRef](#)]
31. Golubov, A.A.; Houwman, E.P.; Gijbertsen, J.G.; Krasnov, V.M.; Flokstra, J.; Rogalla, H.; Kupriyanov, M.Y. Proximity effect in superconductor-insulator-superconductor Josephson tunnel junctions: Theory and experiment. *Phys. Rev. B* **1995**, *51*, 1073–1089. [[CrossRef](#)]
32. Shiota, T.; Imamura, T.; Hasuo, S. Nb Josephson junction with an AlN<sub>x</sub> barrier made by plasma nitridation. *Appl. Phys. Lett.* **1992**, *61*, 1228–1230. [[CrossRef](#)]
33. Kleinsasser, A.W.; Miller, R.E.; Mallison, W.H. Nb/AlN/Nb Josephson Junctions with High Critical Current Density. *IEEE Trans. Appl. Supercond.* **1995**, *5*, 2318–2321. [[CrossRef](#)]
34. Kawamura, J.; Miller, D.; Chen, J.; Zmuidzinas, J.; Bumble, B.; LeDuc, H.G.; Stern, J.A. Very high-current-density Nb/AlN/Nb tunnel junctions for low-noise submillimeter mixers. *Appl. Phys. Lett.* **2000**, *76*, 2119–2121. [[CrossRef](#)]
35. Bumble, B.; LeDuc, H.G.; Stern, J.A.; Megerian, K.G. Fabrication of Nb/Al-N<sub>x</sub>/NbTiN junctions for SIS mixer applications. *IEEE Trans. Appl. Supercond.* **2001**, *11*, 76–79. [[CrossRef](#)]
36. Jackson, B.D.; de Lange, G.; Zijlstra, T.; Kroug, M.; Klapwijk, T.M.; Stern, J.A. Niobium titanium nitride-based superconductor-insulator-superconductor mixers for low-noise terahertz receivers. *J. Appl. Phys.* **2005**, *97*, 113904. [[CrossRef](#)]
37. Karpov, A.; Miller, D.; Rice, F.; Stern, J.A.; Bumble, B.; LeDuc, H.G.; Zmuidzinas, J. Low Noise 1 THz–1.4 THz Mixers Using Nb/Al-AlN/NbTiN SIS Junctions. *IEEE Trans. Appl. Supercond.* **2007**, *17*, 343–346. [[CrossRef](#)]
38. Uzawa, Y.; Fujii, Y.; Gonzalez, A.; Kaneko, K.; Kroug, M.; Kojima, T.; Miyachi, A.; Makise, K.; Saito, S.; Terai, H.; et al. Tuning circuit material for mass-produced terahertz SIS receivers. *IEEE Trans. Appl. Supercond.* **2015**, *25*, 1–5. [[CrossRef](#)]
39. Khudchenko, A.; Baryshev, A.M.; Rudakov, K.I.; Dmitriev, P.M.; Hesper, R.; de Jong, L.; Koshelets, V.P. High-Gap Nb-AlN-NbN SIS Junctions for Frequency Band 790–950 GHz. *IEEE Trans. Terahertz Sci. Technol.* **2016**, *6*, 127–132. [[CrossRef](#)]
40. Shapiro, S. Josephson Currents in Superconducting Tunneling: The Effect of Microwaves and Other Observations. *Phys. Rev. Lett.* **1963**, *11*, 80–82. [[CrossRef](#)]
41. Torgashin, M.Y.; Koshelets, V.P.; Dmitriev, P.N.; Ermakov, A.B.; Filippenko, L.V.; Yagoubov, P.A. Superconducting integrated receiver based on Nb-AlN-NbN-Nb circuits. *IEEE Trans. Appl. Supercond.* **2007**, *17*, 379–382. [[CrossRef](#)]
42. Dmitriev, P.N.; Filippenko, L.V.; Koshelets, V.P. Applications in Superconducting SIS Mixers and Oscillators: Toward Integrated Receivers. In *Josephson Junctions, History, Devices, and Applications*; Wolf, E., Arnold, G., Gurvitch, M., Zasadzinski, J., Eds.; Pan Stanford Publishing Pte: Singapore, 2017; pp. 185–244. ISBN1 978-981-4745-47-5 (Hardcover). ISBN2 978-1-315-36452-0 (eBook).
43. Paramonov, M.E.; Filippenko, L.V.; Dmitriev, P.N.; Fominsky, M.Y.; Ermakov, A.B.; Koshelets, V.P. Parameters of the Tunnel Barrier of Superconducting Niobium-Based Structures. *Phys. Solid State* **2020**, *62*, 1534–1538. [[CrossRef](#)]
44. Simmons, J.G. Generalized Formula for the Electric Tunnel Effect between Similar Electrodes Separated by a Thin Insulating Film. *J. Appl. Phys.* **1963**, *34*, 1793–1803. [[CrossRef](#)]
45. Brinkman, W.F.; Dynes, R.C.; Rowell, J.M. Tunneling conductance of asymmetrical barriers. *J. Appl. Phys.* **1970**, *41*, 1915–1921. [[CrossRef](#)]
46. LeDuc, H.G.; Stern, J.A.; Cypher, S.R. Two-Junction Tuning Circuits for Submillimeter SIS Mixers. *IEEE Trans. Microw. Theory Tech.* **1994**, *42*, 698–706. [[CrossRef](#)]
47. Belitsky, V.Y.; Jacobsson, S.W.; Filippenko, L.V.; Kollberg, E.L. Broadband twin-junction tuning circuit for submillimeter SIS mixers. *Microw. Opt. Technol. Lett.* **1995**, *10*, 74–78. [[CrossRef](#)]
48. Rudakov, K.I.; Dmitriev, P.N.; Baryshev, A.M.; Khudchenko, A.V.; Hesper, R.; Koshelets, V.P. Low-Noise SIS Receivers for New Radio-Astronomy Projects. *Radiophys. Quantum Electron.* **2019**, *62*, 547–555. [[CrossRef](#)]
49. Rudakov, K.I. Development of Advanced Superconductor-Insulator-Superconductor Mixers for Terahertz Radio Astronomy. Ph.D. Thesis, University of Groningen, Groningen, The Netherlands, 2021.
50. Rudakov, K.I.; Koshelets, V.P.; Baryshev, A.M.; Dmitriev, P.N.; Khudchenko, A.V. The 700–950 GHz Superconducting Receiving Structures for Radio Astronomy. *Radiophys. Quantum Electron.* **2017**, *59*, 711–714. [[CrossRef](#)]

51. Khudchenko, A.; Baryshev, A.M.; Hesper, R.; Bekema, M.E.; De, R.; Stijkel, H.; Barkhof, J.; van Nguyen, D.; Koshelets, V.P.; Dmitriev, P.; et al. Performance of SIS mixers for upgrade of CHAMP+ 7-pixel arrays. In Proceedings of the International Symposium on Space Terahertz Technology ISSTT-2017, Cologne, Germany, 13–15 March 2017; pp. 87–90.
52. Otarola, A.; Holdaway, M.; Nyman, L.E.; Radford, S.J.E.; Butler, B.J. Atmospheric Transparency at Chajnantor: 1973–2003, ALMA Memo Series, Memo 512. 2005. Available online: <http://library.nrao.edu/alma.shtml> (accessed on 19 September 2021).
53. Available online: <http://asc-lebedev.ru/index2.php?engdep=16&engsuffa=4> (accessed on 19 September 2021).
54. Available online: <https://www.llamaobservatory.org/en/> (accessed on 19 September 2021).